HELICOPTER AFT-BODY DRAG REDUCTION BY PASSIVE FLOW CONTROL

Moritz Grawunder, Roman Reß, Christian Breitsamter
moritz.grawunder@aer.mw.tum.de
Institute of Aerodynamics and Fluid Mechanics
Technische Universität München

Abstract

The reduction of emissions in air transport is clearly a main goal of the aeronautical industry today, addressing both fixed wing aircraft and rotorcraft. The ADHeRo (Aerodynamic Design Optimization of a Helicopter Fuselage including a Rotating Rotor Head) project contributed to achieving this goal by providing detailed flow characteristics and drag analysis of a state-of-the-art Twin Engine Light (TEL) class utility helicopter with passive flow control devices. This was achieved by means of wind tunnel experiments and numerical simulations.

It has been shown that optimizing the aerodynamic design of the skid-landing-gear is a vital approach for achieving efficiency gains in the twin-engine-light helicopter class. However, further drag reduction potential was identified for the rear fuselage upsweep region. Even though the aerodynamic interference of the modified skid-landing-gear with the fuselage is reduced, it is not entirely eliminated. Thus, the remaining separation at the rear fuselage upsweep provides additional drag reduction potential. Furthermore, the strong lateral tapering of the rear fuselage region also causes the flow to separate from the either side of the fuselage. Delaying this lateral separation also provides drag reduction potential.

Design constraints for the requested rear loading capability do not allow streamlining the aft-body region, i.e. implementing a 'fish-tail' configuration. Thus, the current work is addressing these drag sources through the application of passive flow control devices. The selected devices (strakes and vortex generators) are applied to the rear fuselage upsweep region. In this study counter-rotating vortex generators, simple sheet-metal type strakes and contoured strakes are investigated. This includes a wide experimental analysis of the devices optimal position and their combination. Compared to current production type TEL utility helicopter, the parasite drag could be reduced by another 1.4 - 1.6% in addition to the previous drag savings obtained with the faired skid-landing-gear (21 %).

SYMBOLS

A_{ref}	Reference area	[m^2]
C_D,C_L	Drag and lift coefficient	[-]
F_D,F_L	Drag and lift	[N]
$l_{x,ref}$	Reference length in x-direction	[m]
U_∞	Freestream velocity	[m / s]
α	Angle of attack	[deg]
β	Angle of side slip	[deg]
ρ	Fluid density	[kg / m^3]
ω_x	Axial vorticity	[1 / s]

ABBREVIATIONS

ADHeRo	Aerodynamic Design Optimisation of a Helicopter Fuselage Including a Rotating Rotor Head
GRC	Green Rotorcraft Consortium
SEL	Single-Engine Light
TEL	Twin Engine Light
W/T	Wind Tunnel
AHD	Airbus Helicopters Deutschland GmbH
TUM-AER	Institute of Aerodynamics and Fluid Mechanics at the Technische Universität München
Stereo-PIV	Stereo Particle Image Velocimetry
F0M0	Baseline fuselage and mast fairing
F1M0	Fuselage with smoothed cabin bottom and baseline mast fairing
L0	Baseline skid-landing-gear
L1	Retrofittable faired skid-landing-gear
R0	Rotor Head

1. INTRODUCTION

The presented work is conducted in the framework of the project ADHeRo (Aerodynamic Design Optimization of a Helicopter Fuselage including a Rotating Rotor Head). ADHeRo is a subproject of the Joint Undertaking CleanSky within the Green Rotorcraft Consortium (GRC).

Reducing emissions (CO2, NOX, Noise) is clearly one of the most challenging tasks of the aeronautical industry today. In order to contribute to achieve

efficiency gains for rotorcraft, ADHeRo is aiming to reduce parasite drag for Twin Engine Light (TEL) - class utility helicopters in level flight. In the helicopter fleet from the year 2000, the TEL-class accounted for approximately 10% of the global flight hours performed by civil helicopters [1]. Thus improving the efficiency in the TEL-class can have a relevant impact on the ecological foot print of the global helicopter fleet. For this reason, a state-of-the-art TEL - class utility helicopter with a bearingless main rotor system is subject to the optimisation performed through ADHeRo, see Fig. 1.

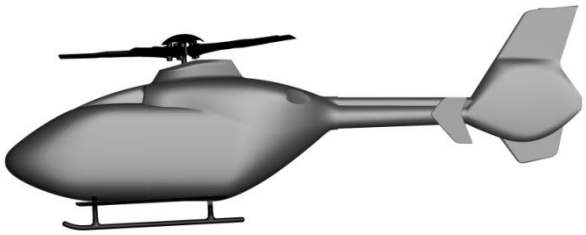

Fig. 1. Investigated state-of-the-art TEL-class utility helicopter [1].

The optimisation is conducted by developing and investigating one baseline and several modified configurations by means of wind tunnel experiments and numerical simulations.

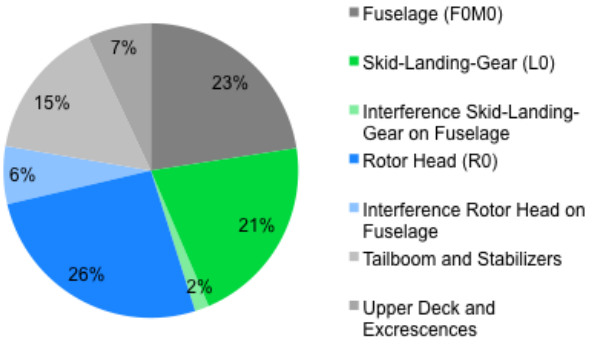

Fig. 2. Drag breakdown of the reference geometry**.**

The authors showed [2] that reducing parasite drag is a viable approach for achieving efficiency gains in the TEL-class. Thus components which contribute the most to parasite drag are improved. Fig. 2 shows that these components are the fuselage, the rotor head and the skid-landing-gear. However, possible changes in the generated down force of the modified components has to be taken into account. Otherwise, the increase in required rotor power (to compensate the additional down force) could deteriorate the achieved efficiency gains. The sensitivity of the total power requirements to changes in down force is much smaller than to changes in drag though. The reason for this is that the rotor acts much more efficiently in generating vertical than horizontal thrust. Thus it is advisable performing a trade-off study before the final selection.

The baseline geometry for the current optimization task is a modified version of the reference geometry depicted in FIG. 1.

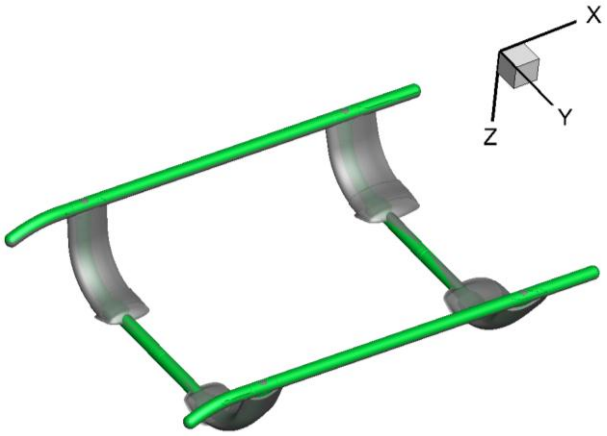

Fig. 3. Faired Skid-Landing-Gear (translucent grey) superimposed on the baseline skid-landing-gear (green).

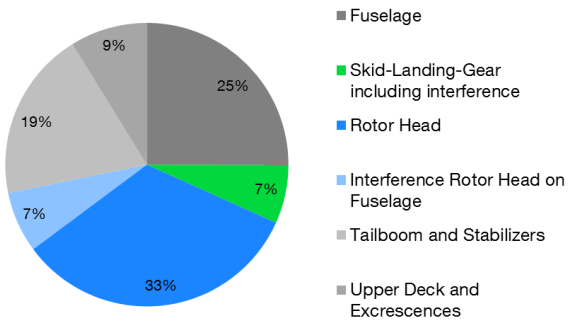

Fig. 4. Reference geometry for the aft-body drag reduction campaign**.**

This modified version features faired skid-landing-gears, see Fig. 3. Compared to the baseline geometry an overall drag reduction of 21 % is achieved with this retrofittable faired skid-landing-gear configuration [3]. However, the faired skid-landing-gear still interferes with the fuselage flow causing additional drag. The drag breakdown of this new configuration shows that the drag associated to the skid-landing-gear form drag and interference drag with the fuselage still accounts for 7 % of the total parasite drag, see Fig. 4. The authors showed that the separation at the rear fuselage upsweep occurs prematurely in the presence of the landing skid. Thus mitigating this interference should yield additional drag savings. Therefore the current analysis is focusing on supressing this separation by passive flow control measures at the rear fuselage. The applied flow control devices include vortex generator, sheet-metal type strakes and contour modifications at the rear fuselage upsweep referred to as contoured strakes.

Applying the strakes is thought to increase the pressure recovery along the lateral tapering at the rear fuselage region. This is achieved by delaying

separation in this region through the deflection of the flow by the presence of the strakes.

The employed vortex generators produce pairs of small scale counter rotating streamwise vortices. This is achieved through the vorticity induced by the counter-rotating vortices. Thus fluid of higher momentum is mixed into the low momentum boundary layer flow. In consequence the flow at the rear fuselage upsweep can withstand a positive pressure gradient longer before separating from the surface. Breitsamter showed that the counter rotating vortex generator type is very efficient in supressing separation [4].

2. MODEL GEOMETRY AND CONFIGURATIONS

The real helicopter geometry, which is to be reproduced using the ADHeRo wind tunnel (W/T) model, represents a characteristic state-of-the-art TEL utility helicopter with a maximum take-off weight of 2.95 metric tons, see Fig. 1. It features a five-bladed bearingless rotor and a backdoor at the rear fuselage upsweep, which is typical for a utility helicopter.

Fig. 5. Baseline configuration of the ADHeRo wind tunnel model (F0M0L0R0).

Fig. 5 depicts the ADHeRo W/T model in its full configuration. The design of the W/T model is primarily driven by the requirement of drag force prediction due to flow separation at the fuselage, skid-landing-gear and rotor head. Thus the tailboom is truncated upstream the empennage allowing for a larger model scale of 1:5. A detailed description of the W/T model design methodology is given in [2].

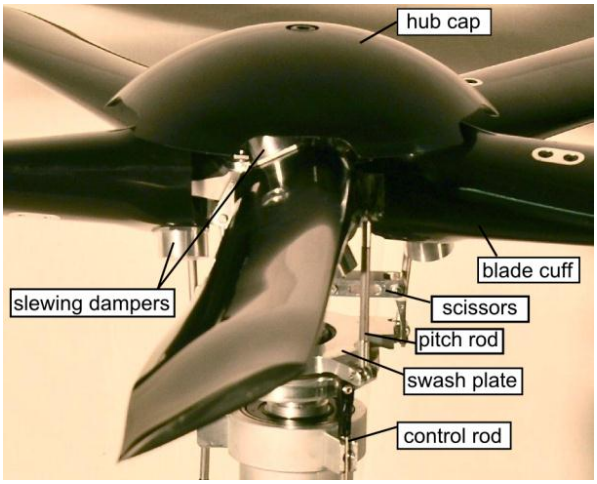

Fig. 6. Detail view of the model rotor head components.

Fig. 6 depicts the design of the W/T model rotor head in detail. As for the other model components, the real helicopter geometry is precisely reproduced on all components exposed to the flow. The model rotor head allows for collective and cyclic pitch motion of the blade cuffs through the application of a fully functional swash blade. The swash blade attitude is fixed at a position that represents the trimmed attitude for the real helicopter configuration in cruising flight. The blade cuffs are truncated at the radial position of the first aerodynamic efficient blade section.

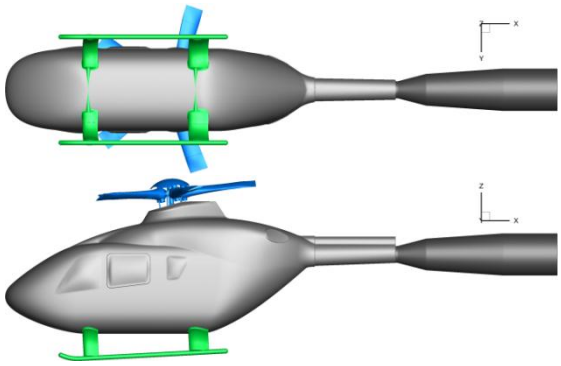

Fig. 7. Baseline configuration for the performed optimization.

The starting point for the current aerodynamic optimization is defined by the geometry depicted in Fig. 7.

2.1. Vortex Generators Geometries and Positions

The vortex generator configuration selected for experiments is based on previous studies performed by Boniface at ONERA [5]. This numerical study investigated the effect of flow control by vortex generators on rear loading ramp drag of the GOAHEAD configuration. The investigated parameter in this study include the location, pitch angle, arrangement (co- or counter-rotating) and the shape of the vortex generator elements. Based on the work of Boniface two vortex generators were selected for the experiments conducted in the framework of the ADHeRo project.

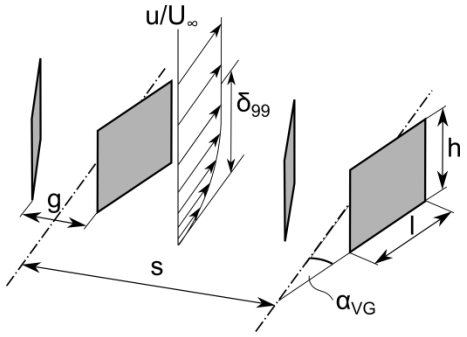

Fig. 8. Two pairs of counter-rotating vortex generators including the geometric parameter for the definition of the studied configurations.

The selected vortex generators are scaled according to the local boundary layer thickness. The local boundary layer thickness δ_{99} = 6 mm is extracted from numerical simulations of the ADHeRo configuration including the faired skid-landing-gear. Based on the conclusions of Boniface only counter-rotating vortex generators are considered, see Fig. 8. The two types of employed vortex generators only deviate from each other in the height h/δ_{99}, featuring values of 0.66 and 1. Thus they are referred to as sub-boundary-layer and boundary-layer scaled vortex generators.

l/δ_{99} [-]	h/δ_{99} [-]	α_{VG} [deg]	g/δ_{99} [-]	s/δ_{99} [-]
3.5	0.66 or 1	15	1.75	5.37

Fig. 9. Vortex generator geometry parameter of the vortex generator employed in experiment depending on the local boundary layer thickness δ_{99}.

Fig. **9** depicts the values for the parameter vortex generator pair gap size g/δ_{99}, length l/δ_{99} and solidity s/δ_{99}. Furthermore, the incidence angle of each vortex generator element α_{VG} is given.

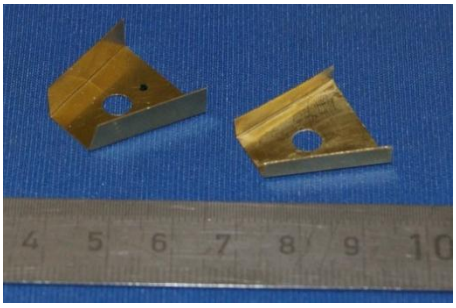

Fig. 10. Vortex generator wind tunnel models made from brass sheet metal of 0.2 mm thickness. Specimen tested in wind tunnel: left) boundary-layer-scaled VG, right) sub-boundary-layer VG.

Fig. 9 depicts the final model scaled vortex generator made from brass sheet metal of 0.2 mm thickness. For experiments the vortex generators are glued to the surface with the connecting base plate. Since the thickness of the sheet metal is minimal, the base plate should not interfere with the flow significantly. In course of the wind tunnel campaign 2 different streamwise positions are investigated. As suggested by Boniface, both streamwise positions are located in the vicinity to the onset of the rear fuselage upsweep. Furthermore, the number of installed counter-rotating vortex generators is varied by installing either 2, 4 or 6 vortex generator pairs. Fig. 11 depicts the relative location of the different vortex generator configurations VG1X0, VG2X0, VG2X20, VG3X20, VG4X20 and VG5. Configuration VG1X0 includes 4 boundary-layer scaled vortex generator pairs, whereas configuration VG2X0 only includes 2 pairs. The suffix X20 of configuration VG2X20 indicates that this configuration sits 20mm further downstream than configuration VG2X0.

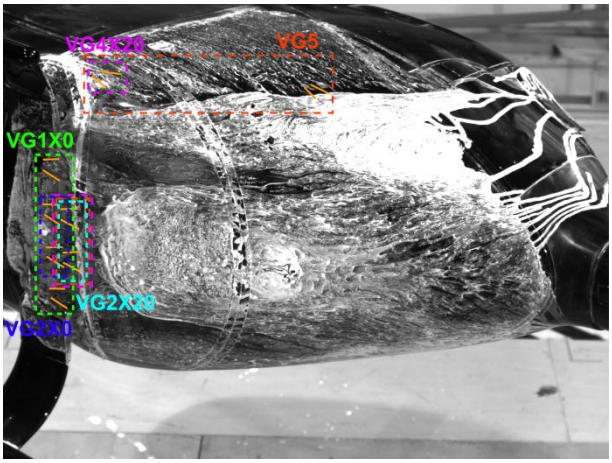

Fig. 11. Vortex generator positions indicated on top of a surface flow visualization of the reference flow topology at zero angle of attack and sideslip.

The vortex generator configuration VG3X20 is the only setup employing the sub-boundary-layer scaled vortex generator. Configurations VG4X20 and VG5 are a combination of 2 vortex generators at the fuselage bottom, equivalent to VG2X20, and 2or 4 vortex generator pairs at the side of the fuselage. These configurations were tested to investigate the potential of the vortex generators in supressing separation at the side of the fuselage too.

2.2. Geometry of the Contoured Strakes

The contoured strakes are provided by the project leader Airbus Helicopter Deutschland GmbH. The contoured strakes, called S10 in this work, are the result of an automated shape optimization performed by Zhang et al. [6]. The procedure is based on a gradient decent approach. The optimization engine calls both the DLR's fluid dynamics solver TAU and the TAU mesh deformation module to calculate the aerodynamics objective function and to change and adapt the surface contour geometry, respectively. In order to reduce the computational costs, gradients are computed by means of TAU's adjoint solver, minimizing the number of functional evaluations.

Fig. 12. Contoured strakes cast silicon parts (red) installed on the ADHeRo wind tunnel model

The set of geometrical boundary conditions only allowed for outbound deflections of the surface. Thus no structural constraints prevent this solution to be retrofitted on production type helicopters. Fig. 12 depicts the resulting shape modifications implemented as cast silicon parts on the ADHeRo wind tunnel model.

2.3. Sheet Metal Type Strakes Geometries and Positions

In course of the wind tunnel campaign 3 different plan form geometries for the sheet metal type strakes are investigated, further called 'simple strakes'. The simple strakes are made from aluminium alloy sheet metal. To attach the simple strakes to the surfaces small angle brackets are screwed to the leeward side of the strakes, see Fig. 13.

Fig. 13. Sheet metal type strakes with mounting brackets.

The base of the angle brackets is glued to the surface and the small gap at the junction of the strake and the surface is sealed with thin sticky tape. The first considered plan form geometry is derived from the shape of the contoured strakes. To achieve this, the line of maximum height along the vertical position is extracted from the contoured strake geometry. Based on this information a first strake element is designed where the local height of the sheet metal element is defined in similarity to this height variation.

Fig. 14. Simple strake S1 installed at the wind tunnel model.

Fig. 14 shows this simple strake, which is described as S1. Strake S1 is positioned along the separation line at the side of the fuselage, see Fig. 15. Strake S1 is mounted not perpendicular to the surface but rather tangential to the sides of the fuselage.

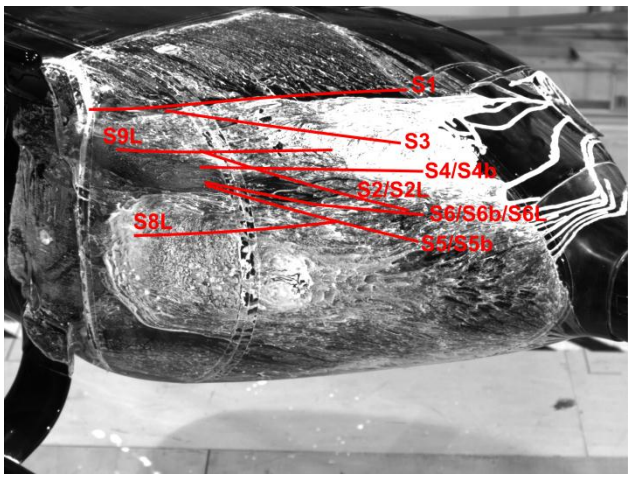

Fig. 15. Sheet metal type strake positions (red lines) indicated on top of a surface flow visualization of the reference flow topology at zero angle of attack and sideslip.

The other two plan form geometries (a) and (b) are shorter compared to strake S1, featuring a length of some 200 mm, see Fig. 16. However, the plan form marked (a) is identical to S1 except that the lower end is truncated. Plan form (b) corresponds in all dimensions except the height to plan form (a). The height of plan form (a) is 25 mm, whereas the height of plan form (b) only amounts to 12 mm. Plan form (a) is employed for the configurations S2, S3, S4, S4b, S5, S5b, S6 and S6 b at the positions indicated in Fig. 15. The difference of those configurations featuring the suffix b is that in this case the strake is not aligned perpendicular to the surface but at an angle of approximately 45 degrees. For configurations S2L, S6L, S8L and S9L the plan form geometry (b) is employed.

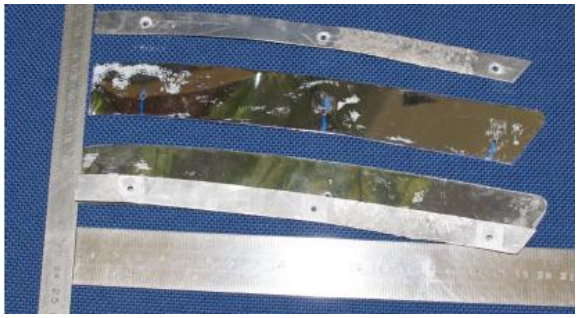

Fig. 16. Different plan form geometries for the sheet metal type strakes. Top: Plan form (b), Centre: Plan form (a), Bottom: Both plan forms in direct comparison.

3. WIND TUNNEL EXPERIMENTS

All W/T experiments conducted within ADHeRo are performed in W/T A at TUM-AER. W/T A is of closed return type and can be operated either in an open or closed test section configuration. For ADHeRo, the test section is always operated in an open configuration, allowing a maximum free stream

velocity U_∞ of 65 m/s. The standard freestream velocity for the ADHeRo measurements is 40 m/s. This corresponds to a freestream Reynolds number Re_∞ of approximately $1 \cdot 10^6$. The freestream Mach number Ma_∞ is 0.1. W/T A provides a freestream turbulence intensity below 0.4 % in all three directions in space.

3.1. Aerodynamic Force Measurements

The global aerodynamic forces and moments acting on the model are recorded with a six-component under-floor W/T balance. All recorded data are time-averaged. Preliminary testing revealed that the measured forces and moments become independent of the integration time for intervals of minimum 15 seconds. Thus this value is chosen for the aerodynamic force and moment measurements performed.

In this paper, all of the force data presented are made dimensionless. The resulting aerodynamic coefficients for drag C_D and lift C_L are assessed through Eq. (1) and (2).

(1) $$C_D = \left(\frac{F_D}{\frac{1}{2}\rho \, {U_\infty}^2 \, A_{ref}} \right)$$

(2) $$C_L = \left(\frac{F_L}{\frac{1}{2}\rho \, {U_\infty}^2 \, A_{ref}} \right)$$

Note that the reference area A_{ref} is kept constant for all investigated configurations to facilitate the comparison of the respective aerodynamic coefficients.

3.2. Stereo Particle Image Velocimetry

Three-dimensional velocity field data is recorded in the wake of the W/T model through the application of Stereo Particle Image Velocimetry (Stereo-PIV). Conventional PIV can only provide two-dimensional velocity vectors within the measuring plane. The employed Stereo-PIV system allows recording the velocity components normal to the measuring plane by exploiting the principles of stereogrametry.

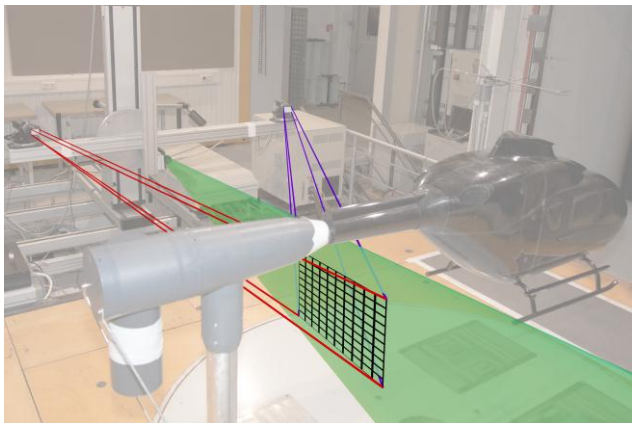

Fig. 17. Stereo PIV measurement setup.

The Stereo-PIV setup employed for ADHeRo is depicted in Fig. 17. For each measurement position 400 data samples are recorded at a sample rate of 15 Hz. The presented velocity data are averaged over all valid data samples.

(3) $$u_{rms} = \left(\frac{1}{n-1} \sum_{i=1}^{n} (u_i - \bar{u})^2 \right)^{\frac{1}{2}}$$

Furthermore, the velocity fluctuations are extracted from the number n of all valid data samples i. The velocity fluctuations in the axial direction are given as root mean square (RMS) values, see Eq. (3).

3.3. Surface Pressure Measurements

In order to gather information about the local flow conditions on the surface of the model, the model is equipped with a pressure measurement system. The system incorporates a combination of steady and unsteady pressure sensors connected to pressure tabs at the model surface. Thus it is possible to record the local surface pressures at each of the pressure tabs during W/T runs. In total, 218 (192 steady and 26 transient) probing positions are equipped with sensors.

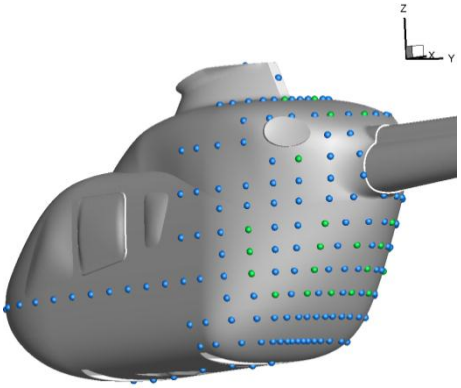

Fig. 18. Pressure probing positions. Steady sensors (blue) and unsteady sensors (green).

Most of the measurement positions are clustered on the aft-body region, thus allowing a precise analysis of the flow around this region of the model. The remaining probing positions are distributed along the centreline and a horizontal section of the model. The sensor array on the W/T model is depicted in Fig. 18. In this paper, only time-averaged pressure distributions are presented. In accordance with the aerodynamic force measurements, the integration time is set to 15 seconds.

Note that no pressure measurements are feasible with the contoured strakes installed. The reason for this is that those strakes are attached to the fuselage as cast silicon parts; thereby most of the pressure probing positions are covered. However, for configurations with vortex generators and sheet metal type strakes the measured pressure distributions are also integrated to estimate the impact on the backdoor drag and lift coefficients.

3.4. Surface Film Visualization Technique

In order to obtain an insight into the effect of the flow control devices on the local near surface flow field a surface film visualization technique is applied. To visualize the near surface flow topology the model is painted with a mixture of paint particles and a solvent before turning on the wind tunnel. When the wind tunnel is turned on the paint particles will move along the local direction of the near surface flow. During this process the solvent slowly evaporates and the paint dries. In consequences the pattern which remains, allows identifying regions of separation, vortex formation and other fluid mechanic phenomenon.

4. Results

Before analyzing the most promising flow control devices and their combinations in detail, an overview over all investigated configurations is given. Fig. 19 depicts for this purpose a block chart presenting the achieved drag reduction as percentage of the reference configuration drag. The reference configuration features the smoothed fuselage with standard mast fairing and faired skid-landing-gear (F1M0L1). Results are shown for angles of attack of 0° and -1.5°, i.e. nose down. The nose down condition is included in this analysis to check the investigated flow control configurations for their sensitivity against variations in the fuselage pitch attitude. Results for configurations increasing the drag level are blanked in Fig. 19. The block chart presents drag reductions from left to right for results of the strake configurations, vortex generator configurations and configurations with combination of the both.

The three most promising strake configurations yield drag reductions in the order of 3 to 4 %. The associated strakes are the simple strakes S2L and S5 and the contoured strakes S10. However, the sensitivity against the fuselage pitch angle differs for these three solutions. For configurations S2L and S10 the sensitivity is small, less than 0.5 %. In contrast, configuration S5 shows a significant sensitivity against the fuselage pitch attitude of slightly over 1 %. The best solution for the strakes only configurations is apparently the configuration with contoured strakes installed. The contoured strakes reduce the drag level of the reference configuration by up to 4 % for the nose down flight attitude. For a neutral pitch attitude this strake solution still yields about 3.5 % drag reduction. The best simple strake solution is configuration S2L. Even though S5 yields similar drag savings for the nose down condition, about 3 %, the sensitivity against variation in fuselage angle of attack is undesirable. Therefore, configurations S2L and S10 are selected from the strake only configurations for further analysis.

From the vortex generator only configurations the highest drag reduction is achieved with some 2 % for the sub-boundary-layer vortex generator configuration VG3X20. However, all vortex generator configurations, except VG2X20, show significant sensitivities against the fuselage pitch attitude. Therefore, the boundary-layer-scaled vortex generator configuration VG2X20, yielding about 1.6 % drag reduction, is selected for further analysis and for studying the effect of a combination of strakes and vortex generators.

Two configurations combining each selected strake solution with the selected vortex generator configuration VG2X20 are investigated. The strake solutions are representing the best solutions found in the strakes only analysis, i.e. S2L and S10. Thus the resulting configurations are termed S2LVG2X20 and S10VG2X20. Comparing the combination S2LVG2X20 against the corresponding strake only configuration shows that the variation with fuselage angle of attack is leveled out by adding the vortex generator VG2X20. Additional drag savings cannot be observed for the combination of vortex generators and simple strakes. For the combination of the vortex generator VG2X20 and the contoured strakes S10, adding the vortex generator decreases the drag by another 0.7 % in comparison to the corresponding strake only configuration. Furthermore, the sensitivity of the achieved drag reduction against the fuselage pitch attitude is also slightly reduced by 0.2 %.

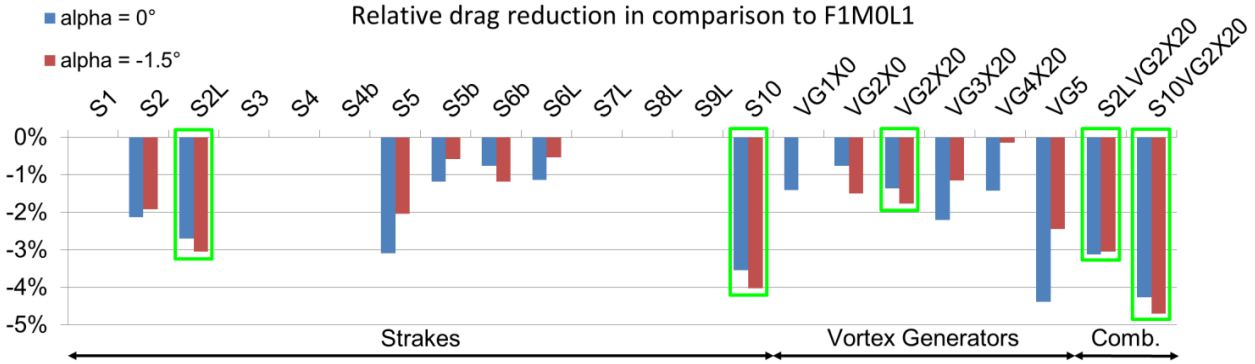

Fig. 19. Achieved relative drag reductions for the employed passive flow control devices in comparison to the reference configuration F1M0L1. Results are shown for angles of attack equal to 0° (blue) and -1.5° (red). Results for configurations with an increased drag level are blanked.

Zhang observed through his numerical simulations that the contoured strakes not only reduce the drag level but also increase the amount of produced lift, see [6]. This would be a desirable effect, since a penalty in lift could deteriorate efficiency gains achieved through drag reduction, see section 0.

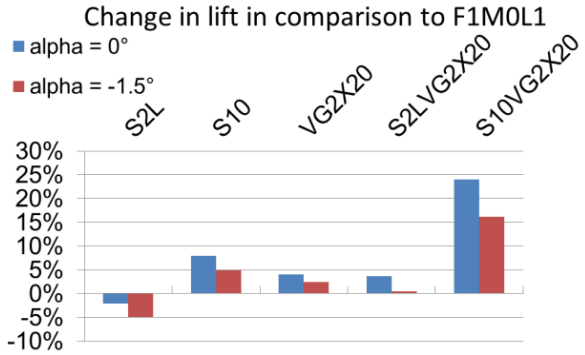

Fig. 20. Change in lift in comparison to the reference configuration F1M0L1 for neutral (blue) and nose down (red) fuselage attitude.

Therefore, the impact on lift of the selected flow control solutions is analyzed. Fig. 20 shows the achieved relative change in lift in comparison to the reference configuration (F1M0L1) for the neutral and nose down fuselage attitude as before. The reference configuration and all selected modified configuration generate down force, thus the relative change in lift has to be considered as a reduction of down force. It is obvious that all selected flow control measures reduce the amount of down force produced except the strake only configurations with the simple strakes S2L installed. What is interesting to note is that the vortex generators are very valuable in reducing the down force. Especially since the effect is magnified when combined with a strake solution. The vortex generators alone reduce the down force by up to 4 %. However, adding them to either of the strake only configuration leads to a reduction of down force of up to 16 %. Hence, combining the strakes with the vortex generators is recommended.

Fig. 21 depicts results for near wall flow topologies for different configurations obtained through a surface film technique in the rear fuselage upsweep region, see section 3.4. The images are recorded always at zero fuselage angle of attack and angle of sideslip. The recorded surface film pictures show the described region looking upstream. Furthermore, the images are rotated by 90° in the clockwise direction to better fit the layout of the paper. Fig. 21 a) presents the near surface flow topology in the rear fuselage upsweep region of the reference configuration. Two distinct features of the flowfield can be identified, the separation in the lower centre region and the separation in the region of lateral tapering of the rear fuselage. Since the convective downstream velocity is significantly reduced through flow separation, or even inversed, the paint particles

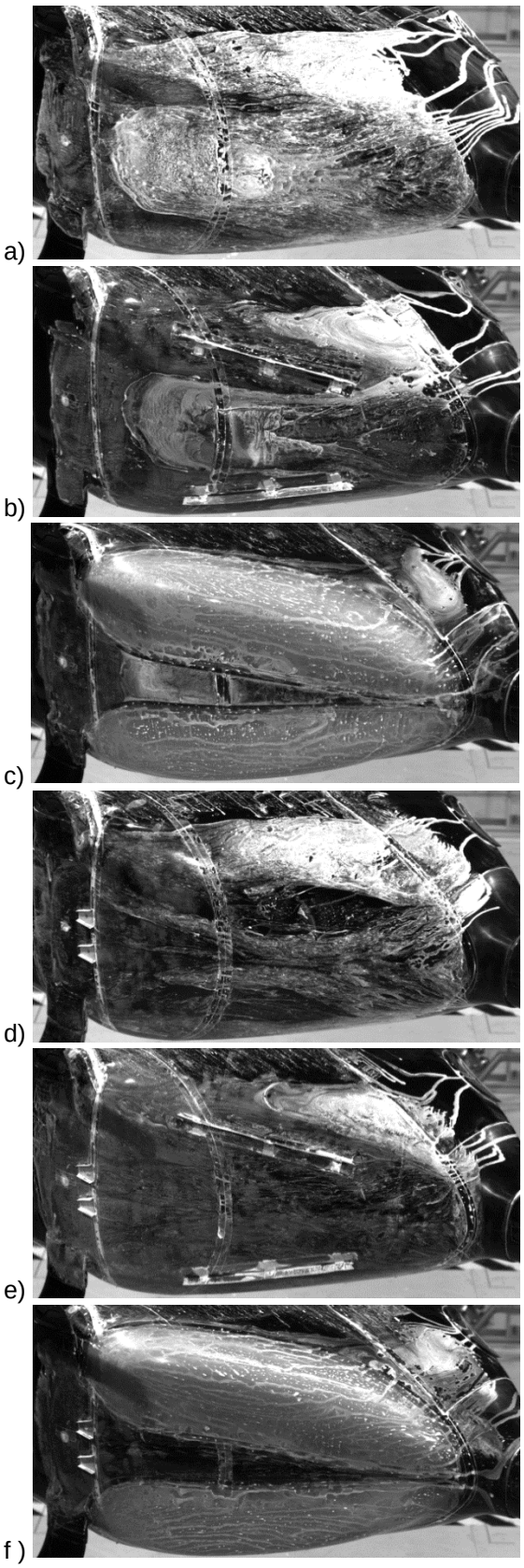

Fig. 21. Surface film visualization of the rear fuselage upsweep near surface flow topology for the a) reference configuration without flow control and with b) S2L, c) S10, d) VG2X20, e) S2LVG2X20 and f) S10VG2X20 installed. The angle of attack and sideslip is set to 0°.

immersed in the surface film are not transported away. In consequence, the particles accumulate in these regions allowing identifying separated flow regimes as intensively coloured spots, white in this case. The intensity varies depending on the amount of paint added to the model before the measurement. Thus the relative variation in colour intensity is indicative in a qualitative sense and not in absolute values. Fig. 21 b) shows the same measurement region but with simple strakes S2L installed. It can be observed that the simple strakes alone already affect both observed separation regions. The separation at the lower centre of the rear fuselage upsweep region becomes narrower in the presence of the simple strakes, whereas the longitudinal position of separation onset remains unchanged. The separation at the lateral tapering is postponed to a more downstream position. Fig. 21 c) shows the surface film result for the strake only configuration with contoured strakes S10. It is observed that the separation at the lateral tapering of the rear fuselage is almost eliminated by modifying the wall contour with the contoured strakes. Apparently the impact on the adverse pressure gradient is significant enough to almost fully supress separation in this region. The central separation at the lower fuselage upsweep also appears to be confined in the lateral direction. Fig. 21 d) presents the results of the surface film visualization for the configuration with vortex generators VG2X20 installed. The effect of the vortex generators of reenergizing the boundary layer to withstand the adverse pressure gradient longer apparently completely supresses the central separation at the lower rear fuselage upsweep. Even the trajectory of the two pairs of counter rotating vortices shedding from the vortex generators downstream can be identified through the applied surface film technique. The separation at the lateral tapering is not affected by the vortex generators VG2X20. From Fig. 21 e) and f) it becomes obvious that supressing the lower central separation is also achieved on the configuration with a combination of strakes and vortex generators by adding the vortex generators. Apparently supressing the lower central separation is the key factor in reducing the down force generated at the fuselage. This is reasonable since the affected fuselage region is inclined against the freestream direction. This naturally transforms changes in the pressure distribution, by supressing separation, not only into drag reductions but also into a reduction of down force as observed.

Fig. 22 depicts contours of surface pressure contours obtained through surface pressure measurements. In order to obtain the surface pressure coefficient contours the pressure coefficients recorded at single data points are interpolated through a Kriging function onto the rear fuselage surface. Please note that the spots of local maxima and minima should not be associated to fluid mechanic phenomena, but rather to partially blocked pressure tabs. Fig. 22 a) depicts the status for the reference configuration F1M0L1. It can be seen that the area with pressure coefficients $c_p > 0$ is already relatively large. However, adding the simple strakes increases the area of positive pressure gradients. The trend observed from the surface film visualization that the separation at the lower centre is becoming narrower in the presence of the simple strakes is confirmed through the obtained pressure contours too; see Fig. 22 b). An impact of the postponed separation at the lateral tapering of the fuselage on the pressure contour cannot be confirmed. Fig. 22 c) depicts the results of the surface pressure contours for the vortex generators only configuration. The supression of the separation at the lower centre of the fuselage is clearly visible also in the pressure contour. In the presence of the vortex generators VG2X20 the area of positive pressure coefficients is clearly extended towards the lower end of the rear fuselage upsweep. Combining both the simple strakes and the vortex generators also shows the best result in the surface pressure distribution; see Fig. 22 d)**.** However, the effect of postponing the separation at the lateral tapering of the fuselage, observed through the surface flow visualization, can be detected for the combined configuration in the pressure distribution as well. The recorded impact on the pressure distribution is comparatively weak though. No results are presented for the pressure distribution in the presence of the contoured strakes. The reason for this is that the contoured strakes, made from silicon cast, cover most of the pressure tabs making pressure measurements unfeasible.

Fig. 23 present results obtained through Stereo-PIV for the reference configuration and the combined configurations with vortex generators and simple or contoured strakes. Results for the downstream velocity deficit are shown in a plane behind the rear fuselage upsweep. The plane location is indicated in the small box in the upper left of each graph. In Fig. 23 a) it can be seen that the size of the velocity deficit region in the wake, corresponds to approximately one third of the fuselage cross section in the region of measurement in the selected downstream plane. For the configuration with vortex generators and simple strakes the velocity deficit in the wake is reduced compared against the reference configuration, see Fig. 23 b). Especially in the lower region of the deficit region the affected area is narrower than before. Furthermore, the maximum deficit is slightly reduced. Thus the observed improvement of the fuselage flow in the presence of the vortex generators and simple strakes is also confirmed through the recorded wake velocity deficit. For the configuration with vortex generators and contoured strakes a similar trend is observed. Both the extension of the wake velocity deficit and the maximum deficit are reduced.

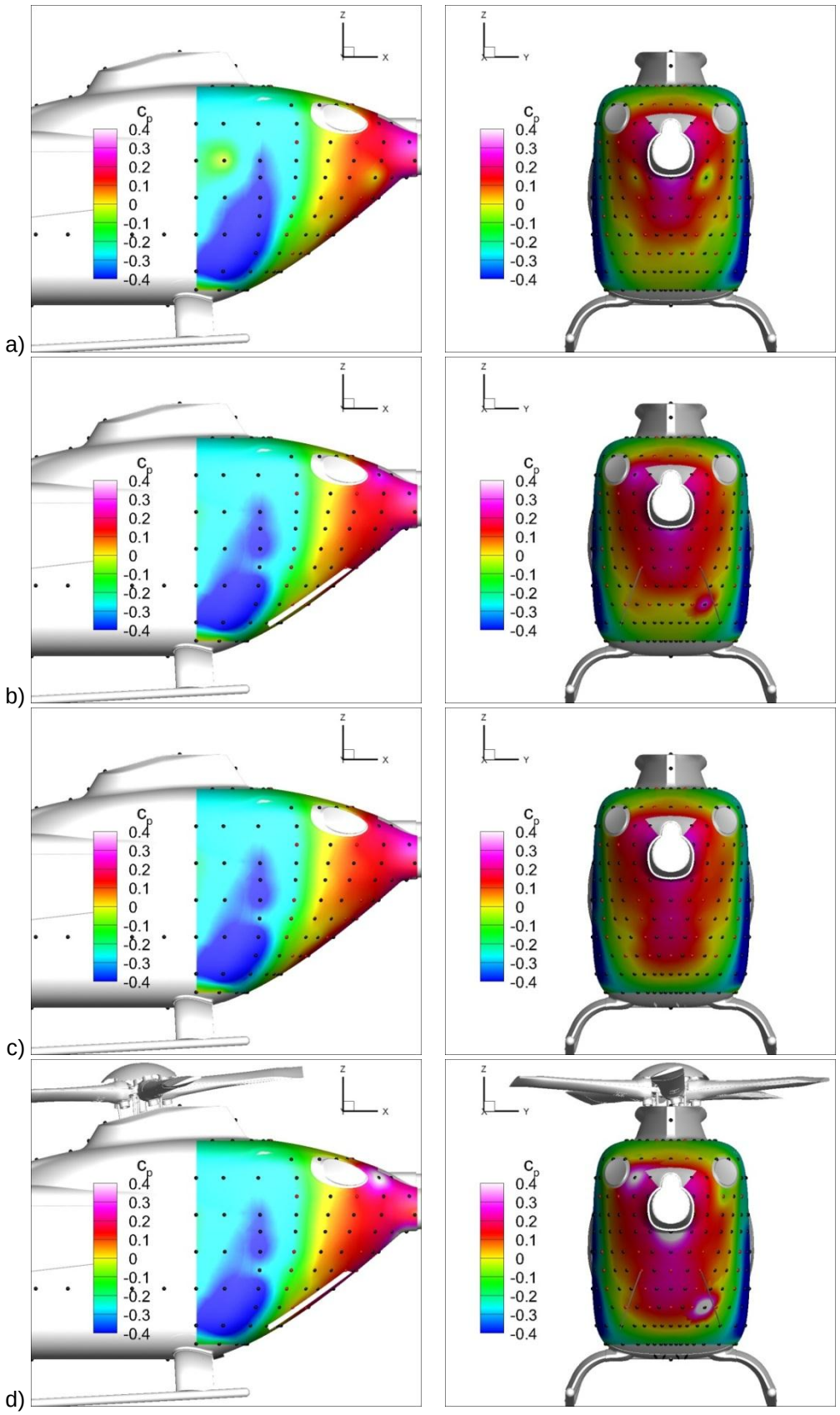

Fig. 22. Static pressure coefficients contours interpolated from the experimental data points (black and red spheres depicted on the surface) onto the rear fuselage region through the application of a Kriging function. The angle of attack and sideslip is set to 0°. a) Reference geometry (F1M0L1), b) strake only configuration S2L, c) vortex generators only configuration VG2X20 and d) combined configuration S2LVG2X20.

However, the structure of the velocity deficit region is changed. Apparently modifying the fuselage shape at the lateral tapering through the contoured strakes reduces the intensity of the upsweep vortices, see [6]. Obviously this also affects the wake velocity deficit region which becomes more compact for the configuration with vortex generators and contoured strakes installed.

5. Conclusions

In the framework of the CleanSky Joint Technology Initiative, the GRC subproject Aerodynamic Design Optimisation of a Helicopter Fuselage including a Rotating Rotor Head (ADHeRo) was initiated in order to increase the aerodynamic efficiency of light-weight rotorcraft. This paper reported on the ADHeRo aft-body flow control campaign. It was conducted to confirm the drag reduction potentials for the application of strakes and vortex generators on a Twin Engine Light (TEL)-class utility helicopter. The aft-body flow control campaign has provided valuable data through the performed wind tunnel experiments. Based on the obtained data set, a detailed study of both global and local flow parameters has been performed.

It was revealed that a significant part of the parasite drag caused by the landing-gear can be obviated through the application of aerodynamic fairings to the skid-landing-gear. However, the interference of the faired skid-landing-gear still accounts for 2 % of the total drag.

Two different combinations of flow control devices were identified, out of 20 configurations, as the most promising solutions for reducing the aft-body drag and the remaining interference effects. Those configurations combine a strake with vortex generators. The configurations deviate by the type of strakes installed. One configuration includes simple sheet metal type strakes whereas the other configuration features contoured strakes. The contoured strakes were developed by the project leader Airbus Helicopters Deutschland GmbH through an automized shape optimization. The selected vortex generators are of the counter rotating type. Two pairs of counter rotating vortex generators positioned at the upsweep line proofed to be the best solution.

The data analysis showed that the configuration with sheet metal type and contoured strakes reduce the fuselage drag by 1.4 % and 1.6 % measured in total parasite drag of the real helicopter, respectively. The performed surface pressure and surface film measurements allowed identifying the source of the achieved drag reduction. Both types of considered strakes delay the separation at the lateral tapering of the rear fuselage. Furthermore, the strakes influence the separation at the lower centre of the rear fuselage upsweep. However, the application of the vortex generators proofed to be necessary to fully supress the separation in this region.

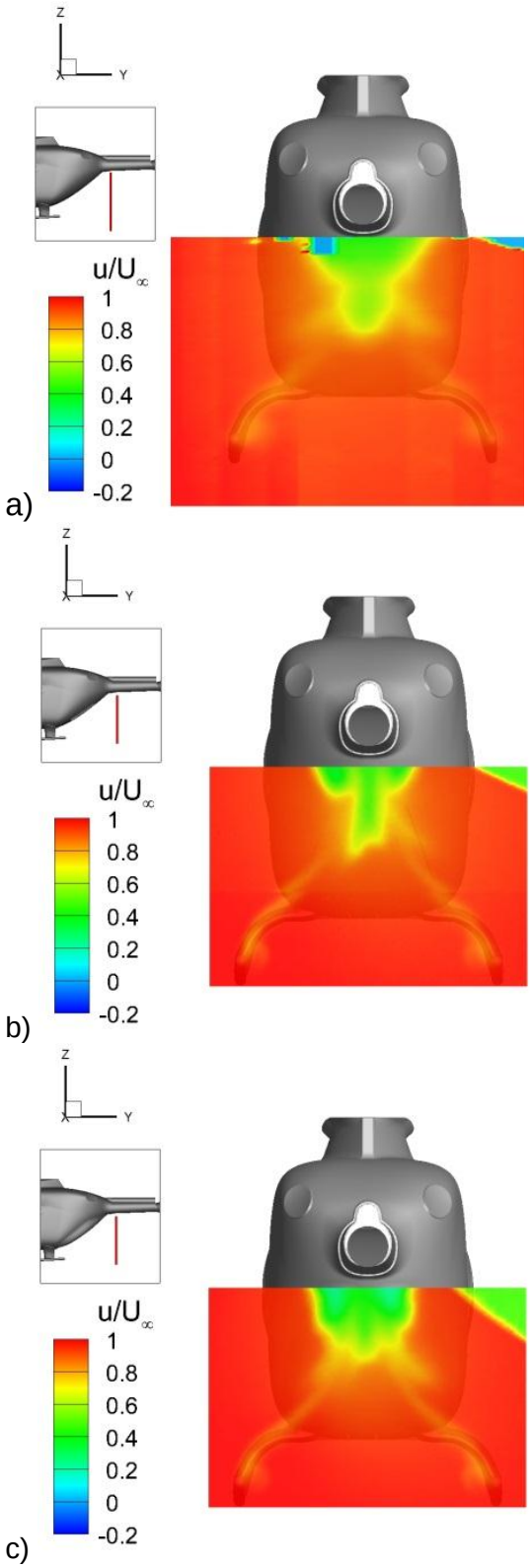

Fig. 23. Contours of downstream velocity deficit obtained through Stereo-PIV in a plane downstream of the rear fuselage upsweep. The downstream position of the measurement plane is shown on the upper left of each graph. The angle of attack and sideslip is set to 0°. a) Reference configuration, b) configuration with simple strakes and vortex generators and c) configuration with contoured strakes and vortex generators.

Measuring the velocity deficit in the wake with Stereo Particle Image Velocimetry confirmed the positive effect of selected flow control devices. Both configurations with flow control devices featured a reduced extension of the wake velocity deficit region and a reduced maximum velocity deficit.

ACKNOWLEDGMENTS

The research leading to these results received funding from the European Community's Seventh Framework Program (FP/2007-2013) for the Clean Sky Joint Technology Initiative under grant agreement number 270563. The authors would like to thank the project leader Airbus Helicopters Deutschland GmbH for the fruitful collaboration and valuable support. Furthermore, special thanks are addressed to ANSYS CFX for providing the flow simulation software. The work of our student Stephanie Müller is also highly appreciated.

REFERENCES

[1] Airbus Helicopters Germany GmbH

[2] Grawunder, M. et al.: Flow Characteristics of a Helicopter Fuselage Configuration Including a Rotating Rotor Head. 28th International Congress of the Aeronautical Sciences, Brisbane (2012)

[3] Grawunder, M. et. al.: Optimized Skid-Landing-Gears for Twin-Engine-Light Utility Helicopter. 39th European Rotorcraft Forum, Moscow (2013)

[4] Breitsamter, C.: Innovative High-Lift concepts of the integrated research programs AWIATOR and IHK, Luftfahrttechnisches Handbuch (LTH), AD-04-02-004, Mai 2009, pp. 1-50.

[5] Boniface, J.: A Computational Framework for Helicopter Fuselage Drag Reduction Using Vortex Generators. American Helicopter Society 70th Annual Forum, Québec (2014)

[6] Zhang, Q. et al.: Advanced CFD-based Optimization Methods Applied to the Industrial Design Process of Airframe Components at Airbus Helicopters. American Helicopter Society 70th Annual Forum, Québec (2014)

CLASSIFICATION & COPYRIGHT